The Astrophysical Journal Letters, 923:L3 (8pp), 2021 December 10 https://doi.org/10.3847/2041-8213/ac3a0e

Absolute Absorption Cross Section and Orientation of Dangling OH Bonds in Water Ice

Takumi Nagasawa[1], Reo Sato[1], Takeshi Hasegawa[1], Naoki Numadate[1], Nobutaka Shioya[2], Takafumi Shimoaka[2], Takeshi Hasegawa[2], and Tetsuya Hama[1,3]
[1] Komaba Institute for Science and Department of Basic Science,The University of Tokyo, Meguro, Tokyo 153-8902, Japan; hamatetsuya@g.ecc.u-tokyo.ac.jp
[2] Institute for Chemical Research, Kyoto University, Uji, Kyoto 611-0011, Japan
Received 2021 October 1; revised 2021 November 4; accepted 2021 November 15; published 2021 December 6

Abstract

The absolute absorption cross section of dangling OH bonds in water ice, a free OH stretch mode by three-coordinated surface water molecules, is derived experimentally as $1.0 \pm 0.2 \times 10^{-18}$ cm^2 at 3696 cm^{-1} for amorphous water at 90 K using infrared multiple-angle incidence resolution spectrometry (IR–MAIRS). The integrated absorption cross section (band strength) of the dangling OH bond at 90 K ($1.4 \pm 0.3 \times 10^{-17}$ cm molecule^{-1} at 3710–3680 cm^{-1}) is found to be more than 1 order of magnitude smaller than those in bulk ice or liquid water. This indicates that a lack of hydrogen-bonding significantly decreases the band strength of dangling OH bonds. The present study also provides average molecular orientations of dangling OH bonds at 10 K and 90 K, because both the surface-parallel (in-plane) and surface-perpendicular (out-of-plane) vibration spectra of dangling OH bonds are quantitatively measured by IR–MAIRS. The intensity ratio of the dangling-OH peaks between in-plane to out-of-plane spectra shows the isotropic nature (random orientation) of the two- and three-coordinated dangling OH bonds in microporous amorphous water prepared at 10 K; however, the three-coordinated dangling OH bonds in nonporous amorphous water prepared at 90 K are dominantly located at the top ice surface and oriented perpendicular to it. These findings provide fundamental insights into the relationship between the structure and optical properties of ice surfaces, and aid quantitative understanding of the surface structure of interstellar ices and their laboratory analogs.

Unified Astronomy Thesaurus concepts: Interstellar dust (836); Interstellar molecules (849); Ice formation (2092); Laboratory astrophysics (2004); Interdisciplinary astronomy (804); Experimental techniques (2078); Surface ices (2117)

1. Introduction

Infrared (IR) observations of space have revealed that water (H_2O) ice is the most abundant solid component of cold interstellar clouds, the birthplaces of stars and planets (Van Dishoeck et al. 2013). Most of this ice is considered to be amorphous because of the lack of a sharp OH-stretching feature around 3200 cm^{-1} (3.1 μm) that is characteristic of four-coordinated molecules in crystalline ice (Hama & Watanabe 2013; Van Dishoeck et al. 2013). Laboratory IR spectra of microporous amorphous water prepared at low temperatures instead show two weak features at 3696 and 3720 cm^{-1}, which have been, respectively, assigned to the free OH stretching modes of three-coordinated (one hydrogen (H)-donor and two H-acceptors) and two-coordinated (one H-donor and one H-acceptor) molecules located at the ice surface; these are often called dangling OH bonds (Buch & Devlin 1991; Devlin & Buch 1995). As dangling OH bonds indicate the porosity of ice while acting as sites of preferential adsorption and reaction on the ice surface, extensive studies have sought to understand the surface properties of interstellar ice and its catalytic role in the formation of molecules in space (Stevenson et al. 1999; Hama & Watanabe 2013; He et al. 2019; Noble et al. 2020). Although the dangling OH features have yet to be observed in the IR spectra of interstellar ices (Van Dishoeck et al. 2013), the upcoming James Webb Space Telescope will search for them with high sensitivity and high spectral and spatial resolution, thus shedding light on interstellar ice surface structures (Gorai et al. 2020).

Despite much active research, the absorption cross section of dangling OH bonds remains unknown (as explained below), which hinders quantification of these bonds. Beer's law (Equation (1)) gives a sample's absorbance (A) and absorption cross section (σ, cm^2) as a function of the imaginary part of its complex refractive index, ($n_2 + ik_2$).

$$A = -\log_{10}\frac{S^s}{S^b} = \frac{\sigma N}{\ln 10} = \frac{4\pi d k_2}{\lambda \ln 10}, \quad (1)$$

where S is the intensity of the transmitted IR light of wavelength λ (μm), and the superscripts s and b indicate background and sample measurements, respectively (Hasegawa 2017). The sample has thickness d (μm) and column density N (molecules cm^{-2}). An often overlooked aspect of Beer's law is its neglect of optical interfaces (e.g., sample–substrate interface); it thus holds only for a bulk sample thicker than the IR wavelength ($d \geqslant \lambda$) (Hasegawa 2017). However, laboratory measurements of H_2O ice at low temperature in vacuum typically use ice thinner than hundreds of nanometers: i.e., $d \ll \lambda$ (Hagen et al. 1981; Mastrapa et al. 2009). In such cases, the thin sample's absorbance is induced by the electric field at optical interfaces (vacuum–sample–substrate interfaces) different from the far field (Hasegawa 2017). Itoh et al. deduced from Maxwell's equations an analytical expression for the absorbance of a thin sample in a typical, five-layer, symmetric

[3] Author to whom correspondence should be addressed.

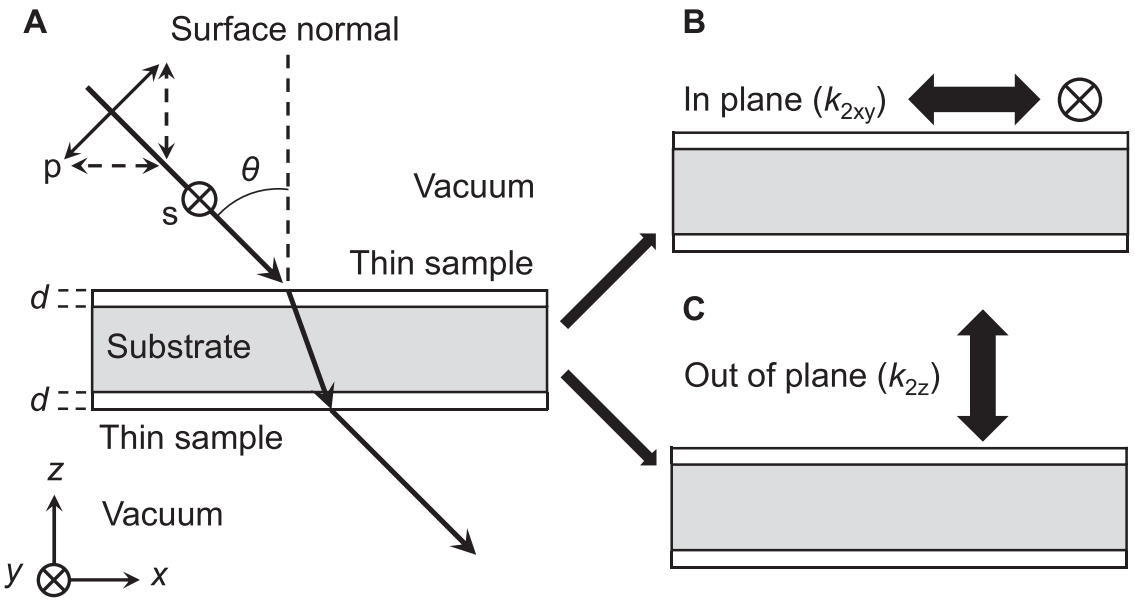

Figure 1. IR–MAIRS measurement system. Panel (A): Oblique incidence transmission measurements in a five-layer system (vacuum/thin sample/substrate/thin sample/vacuum). d is the thickness of the thin sample. θ is the angle of incidence. Solid double-headed arrow shows the direction of the electric field vector for p-polarized radiation, which can be divided into x- and z-direction components (dashed double-headed arrows). $\otimes$ shows the direction of the electric field vector for the s-polarized radiation (i.e., the y-direction). IR–MAIRS collects IR spectra of the thin sample at $\theta = 45°$ with seven polarization angles (ϕ) from s-polarization ($\phi = 0°$) to p-polarization ($\phi = 90°$) in 15° steps. Panels (B) and (C): Pure IP (k_{2xy}) and OP (k_{2z}) spectra are calculated using classical least-squares regression (see also the Appendix for details).

double-sided vapor-deposited ice system (vacuum/thin sample/IR-transparent substrate/thin sample/vacuum) used in laboratory studies (Itoh et al. 2009). They expressed the absorbance of a thin sample for normal incidence using linearly polarized IR light ($A_{\text{thin}}^{\theta=0}$) as follows:

$$A_{\text{thin}}^{\theta=0} = -\log_{10}\frac{S^s}{S^b} = \frac{8\pi da}{\lambda \ln 10}(2n_2k_{2xy}) \tag{2}$$

$$a = \frac{1}{n_1+n_3} + \left(\frac{n_1-n_3}{n_1+n_3}\right)^4 \times \left\{1-\left(\frac{n_1-n_3}{n_1+n_3}\right)^4\right\}^{-1}\left(\frac{2n_3}{n_3^2-n_1^2}\right), \tag{3}$$

where n_1 and n_3 are the refractive indices of vacuum and the substrate, respectively; the coefficient a expressed by n_1 and n_3 results from the optical interface effects and k_{2xy} is the x- and y-components of the imaginary part of the complex refractive index of the thin sample (Figure 1 defines the x-, y-, and z-directions). A uniaxial system ($k_{2x} = k_{2y} = k_{2xy}$) is assumed here for simplicity, and k_{2xy} and k_{2z} (z-component) are related to optically isotropic k_2 in Equation (1) as follows (Shioya et al. 2020):

$$k_2 = \frac{2k_{2xy}+k_{2z}}{3}. \tag{4}$$

In contrast to the bulk absorbance, A in Equation (1), $A_{\text{thin}}^{\theta=0}$ is influenced by n_1, n_2, and n_3 as shown in Equations (2) and (3). Supporting this, a clear correlation between the absorbance of organic thin film ($A_{\text{thin}}^{\theta=0}$) and the substrate's refractive index (n_3) has been reported (Umemura et al. 1990). In addition, $A_{\text{thin}}^{\theta=0}$ contains the transverse optic (TO) energy-loss function of the thin sample ($2n_2k_{2xy}$). This means that only the surface-parallel (in-plane, IP) vibration is observed in the IR spectrum of a thin sample, without the surface-perpendicular (out-of-plane, OP) vibration given by k_{2z} (Umemura et al. 1990; Itoh et al. 2009; Hasegawa 2017; Hasegawa & Shioya 2020). However, σ requires by definition the isotropic k_2 in Equation (1), meaning that it is inaccurate to calculate σ from the IR spectrum of thin H_2O ice measured using conventional normal-incidence transmission. To measure σ for dangling OH bonds, it is necessary to measure both k_{2xy} and k_{2z}, correct the optical interface effects expressed by n_1, n_2, and n_3, and obtain the isotropic k_2.

Here, we report experimental IR multiple-angle incidence resolution spectrometry (IR–MAIRS) measurements of σ for dangling OH bonds in amorphous water (Figure 1 and see also the Appendix for details). IR–MAIRS is a spectroscopic method combining oblique incidence transmission measurements and multivariate analysis to retrieve both pure in plane (IP) (k_{2xy}) and out of plane (OP) (k_{2z}) vibration spectra for a thin sample. It was originally developed for quantitative molecular orientation analysis of organic thin films without the use of optical parameters (Shioya et al. 2019; Hama et al. 2020; Hasegawa & Shioya 2020). This study employs IR–MAIRS to measure the IP and OP spectra of dangling OH bonds in amorphous water, and derive the absolute value of σ without the contributions of n_1, n_2, and n_3 based on analytical expressions for the IP and OP spectra.

2. Results and Discussion

We first verified the detectability by IR–MAIRS of dangling OH bonds in microporous amorphous water (Stevenson et al. 1999; Hama & Watanabe 2013; He et al. 2019; Noble et al. 2020). In this study, amorphous water samples were prepared

using H_2O with 3.5 mol% HDO to allow measurement of the OD stretching vibration decoupled from intramolecular and intermolecular OH stretching vibrations (Franks 1972; Klug et al. 1987; Hama et al. 2017). The decoupled OD stretching vibration band was used to validate the IR–MAIRS measurements and analysis in the present study (see the Appendix for details). The contribution of the surface HDO molecules to dangling OH bonds should be negligible considering its small concentration of 3.5 mol%.

Figure 2(A) shows the IP and OP spectra of dangling OH bonds in microporous amorphous water on a Si substrate at 10 K as a function of gas exposure time. The pressure in the chamber is 2.2×10^{-6} Pa during water exposure (for details, see the Appendix). Both spectra include two peaks at 3720 and 3696 cm^{-1} for dangling OH in two- and three-coordinated molecules, respectively. Both peaks' band intensities increased as the ice thickness increased during gas deposition over 32–128 minutes; this trend is characteristic of the formation of microporous amorphous water having a large internal surface area. Stevenson et al. showed that amorphous water becomes increasingly porous with decreasing deposition temperature $\leqslant$77 K: their N_2 adsorption measurements showed an apparent surface area of 2700 $m^2\ g^{-1}$ at 22 K versus 640 $m^2\ g^{-1}$ at 77 K (Stevenson et al. 1999). Similar band shapes and intensities between the IP and OP spectra at 10 K at each exposure time for 32–128 minutes indicate the isotropic nature (random orientation) of the dangling OH bonds in the internal pore surface (Hama et al. 2020; Hasegawa & Shioya 2020; Shioya et al. 2020).

Overlap of the two dangling OH peaks complicates the measurement of σ. Therefore, we prepared nonporous amorphous water by vapor deposition at 90 K; it exhibited only the three-coordinated dangling-OH peak (Bahr et al. 2008; Hama & Watanabe 2013; Bu et al. 2015; He et al. 2019). The OP and IP spectra in Figure 2(B) show no peak at 3720 cm^{-1} for two-coordinated molecules at 90 K; however, the OP spectra includes the peak at 3696 cm^{-1} for three-coordinated molecules. The corresponding IP spectra does not show this peak. The peak's intensity in the OP spectra remain constant at each exposure time for 32–128 minutes (Figure 2(C)). These results suggest that three-coordinated dangling OH bonds in nonporous amorphous water at 90 K are located at the top ice surface and oriented perpendicular to it. We also confirm that the peak at 3696 cm^{-1} is invisible using normal-incidence transmission at 90 K (Figure 2(C)), supporting that IR–MAIRS is required to measure σ.

The number density of three-coordinated dangling-OH bonds at 90 K is estimated using methanol (CH_3OH) deposition because it creates hydrogen bonds with dangling OH bonds and quenches the peak at 3696 cm^{-1} (Bahr et al. 2008). Figure 3(A) shows the disappearance of this peak during CH_3OH deposition at $2.2 \pm 0.2 \times 10^{-8}$ Pa, which corresponds to a flux of $7.8 \pm 0.9 \times 10^{10}$ molecules $cm^{-2}\ s^{-1}$. The dangling-OH peak at 3696 cm^{-1} decreases after 2.5 minutes of deposition, and completely vanishes after 6.5 minutes. In addition, a new peak for the CO stretching band of CH_3OH appears at 1033 cm^{-1} only in the OP spectra after CH_3OH deposition (Figure 3(B)). This result indicates that the CO stretching band of CH_3OH has a strong perpendicular orientation to the amorphous water surface plausibly by hydrogen-bond formation with the three-coordinated dangling OH bonds (Dawes et al. 2016).

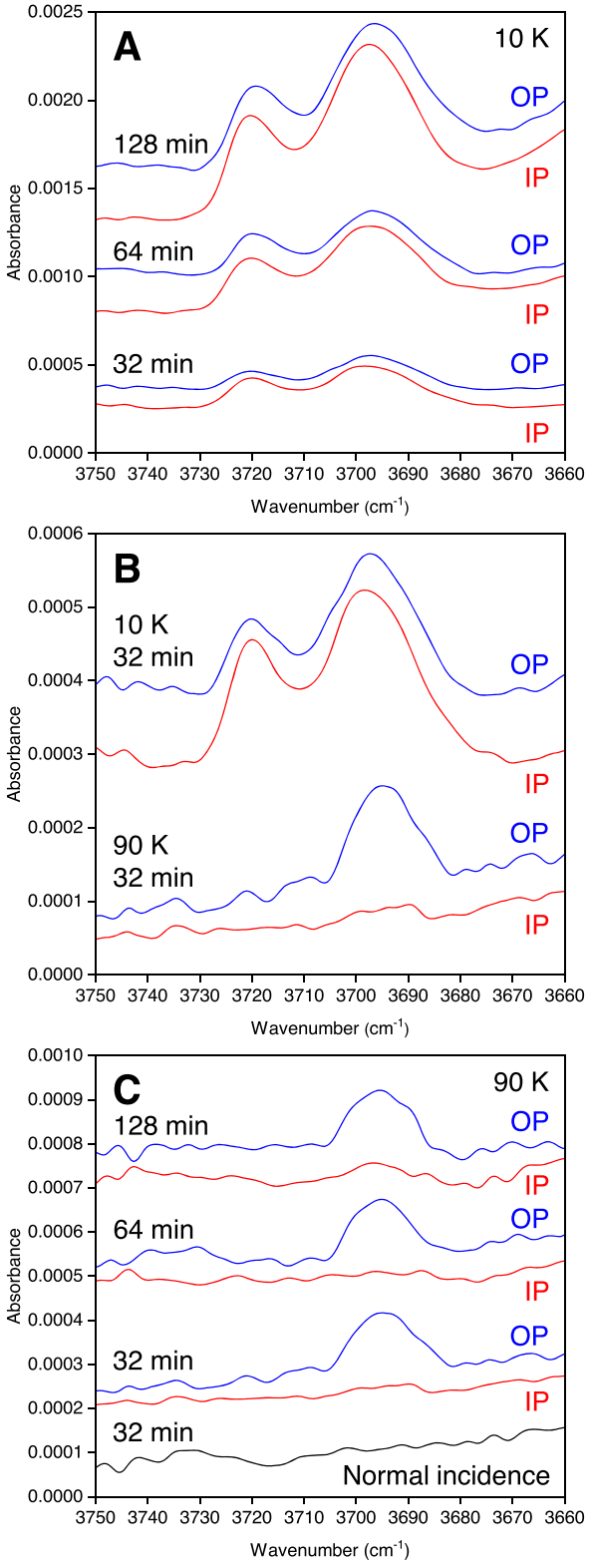

Figure 2. IP and OP spectra of amorphous water on a Si substrate at 3750–3660 cm^{-1}. (A) Amorphous water at 10 K as a function of water exposure time. (B) Amorphous water at 10 K and 90 K formed after 32 minutes of water exposure. (C) Amorphous water at 90 K as a function of water exposure time. Bottom black line in (C) shows normal-incidence IR spectrum ($\theta = 0°$, $\phi = 90°$) for amorphous water formed after 32 minutes of water exposure. The pressure in the chamber is 2.2×10^{-6} Pa during water exposure. The amorphous water samples were prepared using H_2O with 3.5 mol% HDO (see the Appendix for details).

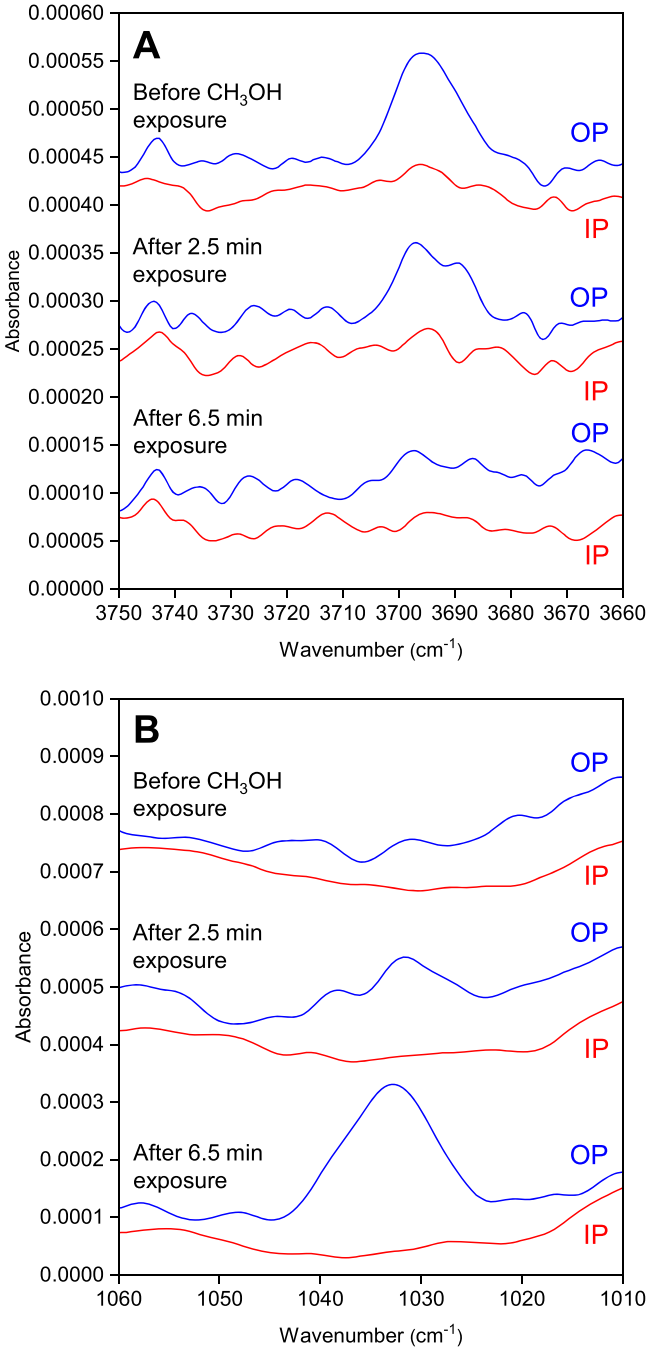

Figure 3. IP and OP spectra of amorphous water on a Si substrate at 90 K as a function of CH_3OH exposure time. (A) 3750–3660 cm^{-1} for the dangling-OH peak and (B) 1060–1010 cm^{-1} for the CO stretching band of CH_3OH. Amorphous water was prepared at 90 K by 32 minutes of water exposure (H_2O with 3.5 mol% HDO) at 2.2×10^{-6} Pa before CH_3OH exposure. The pressure in the chamber is 2.2×10^{-8} Pa during CH_3OH exposure.

Bahr et al. assigned the peak at 1034 cm^{-1} to CH_3OH species directly interacting with the amorphous water surface by hydrogen-bonding (Bahr et al. 2008). Repeated experiments show that CH_3OH deposition for 6.5 ± 0.5 minutes is required to fully quench the peak. This corresponds to an exposure of $3.1 \pm 0.4 \times 10^{13}$ molecules cm^{-2} s^{-1}. We also calculated the amount of CH_3OH adsorbed on the amorphous water surface as $3.5 \pm 0.4 \times 10^{13}$ molecules cm^{-2} from the CO stretching band area at 1050–1020 cm^{-1} in the OP spectra using the band strength of 1.59–1.69 $\times$ 10^{-17} cm molecule^{-1} (Luna et al. 2018), which is in good agreement with the amount of CH_3OH exposure (for details, see the Appendix). Based on these results, we estimate the number density of three-coordinated dangling-OH bonds at 90 K as $3.3 \pm 0.6 \times 10^{13}$ molecules cm^{-2}.

Analytical expressions for the IP and OP spectra obtained by IR–MAIRS are theorized by Itoh et al. (2009) and Shioya et al. (2019). In short, Shioya et al. showed both experimentally and theoretically that the IP spectrum (A_{IP}) quantitatively corresponds to the normal-incidence transmission spectrum, $A_{thin}^{\theta=0}$ (see the Appendix for details; Shioya et al. 2019).

$$A_{IP} = A_{thin}^{\theta=0} = \frac{8\pi da}{\lambda \ln 10}(2n_2 k_{2xy}). \tag{5}$$

A_{OP} is expressed similarly to A_{IP}, while the TO energy-loss function is replaced with a longitudinal optic (LO) energy-loss function: i.e., $(2n_2k_{2z})/(n_2^2 + k_{2z}^2)^2$ (Shioya et al. 2019; Hama et al. 2020).

$$A_{OP} = \frac{8\pi da}{H\lambda \ln 10}\frac{(2n_2 k_{2z})}{(n_2{}^2 + k_{2z}{}^2)^2}, \tag{6}$$

where H is a substrate-specific correction factor (0.33 for Si) that accounts for the intensity ratio of the electric fields at the optical interface along the surface-parallel and surface-perpendicular directions (Shioya et al. 2019). Because amorphous H_2O vapor-deposited at 80–100 K has values of k_2 that are approximately 2 orders of magnitude smaller than n_2 ($k_2 \ll n_2$) at 3750–3650 cm^{-1} in the bulk (Mastrapa et al. 2009), Equation (6) simplifies to

$$A_{OP} \approx \frac{8\pi da}{H\lambda \ln 10}\frac{(2n_2 k_{2z})}{n_2{}^4}. \tag{7}$$

From Equations (5) and (7), k_{2xy} and k_{2z} are derived as

$$k_{2xy} = \frac{A_{IP}\lambda \ln 10}{16\pi dan_2} \tag{8}$$

$$k_{2z} = \frac{n_2{}^4 H A_{OP}\lambda \ln 10}{16\pi dan_2}. \tag{9}$$

Therefore, optically isotropic k_2 and σ can be obtained from A_{IP} and A_{OP} even for a thin sample (Shioya et al. 2020):

$$\begin{aligned} k_2 &= \frac{2k_{2xy} + k_{2z}}{3} \\ &= \left(\frac{2A_{IP} + n_2{}^4 H A_{OP}}{3}\right)\frac{\lambda \ln 10}{16\pi dan_2} \end{aligned} \tag{10}$$

$$\begin{aligned} \sigma &= \frac{4\pi dk_2}{\lambda N} \\ &= \frac{4\pi d}{\lambda N}\left(\frac{2A_{IP} + n_2{}^4 H A_{OP}}{3}\right)\frac{\lambda \ln 10}{16\pi dan_2} \\ &= \left(\frac{2A_{IP} + n_2{}^4 H A_{OP}}{3}\right)\frac{\ln 10}{4an_2 N}. \end{aligned} \tag{11}$$

Table 1
Summary of Band Strengths [cm molecule^{-1}] for Water

Species	Band strength (wavenumber range)
Dangling OH at 90 K (This study)	$1.4 \pm 0.3 \times 10^{-17}$ (3710–3680)
Dangling OH (Calculation) (Maté et al. 2021)	1.2×10^{-17} (3700–3640)
Amorphous water at 80 K (Mastrapa et al. 2009)	2.9×10^{-16} (4320–2956)
Crystalline ice at 267–273 K[a] (Schaaf & Williams 1973)	2.3×10^{-16} (3900–2700)
Liquid water at 295–298 K[a] (Max & Chapados 2009)	1.5×10^{-16} (3900–2700)
Monomer in solid CO at 10 K (Ehrenfreund et al. 1996)	1.1×10^{-17} (3707)[b]
Monomer in solid N_2 at 10 K (Ehrenfreund et al. 1996)	7.8×10^{-18} (3726)[b]
Monomer in solid O_2 at 10 K (Ehrenfreund et al. 1996)	3.3×10^{-18} (3732)[b]

Notes.
[a] See the Appendix for details of the band strength calculations for crystalline ice and liquid water.
[b] Asymmetric OH stretching vibration.

The band strength β (cm molecule^{-1}) can be also obtained by integrating $\sigma(\tilde{\nu})$ at $\tilde{\nu}$= 3710–3680 cm^{-1}.

$$\beta = \int \sigma(\tilde{\nu}) d\tilde{\nu} = \left(\frac{2}{3} \int A_{\rm IP}(\tilde{\nu}) d\tilde{\nu} + \frac{{n_2}^4 H}{3} \int A_{\rm OP}(\tilde{\nu}) d\tilde{\nu} \right) \frac{\ln 10}{4 a n_2 N}, \quad (12)$$

where $A_{\rm IP}(\tilde{\nu})$ and $A_{\rm OP}(\tilde{\nu})$ is the IP and OP absorbance at a given wavenumber ($\tilde{\nu}$), respectively. This study uses $n_1 = 1$ for vacuum, $n_2 = 1.26$ for amorphous water at 90 K (Kofman et al. 2019), and n_3=3.41 for Si (Tasumi 2014; Shioya et al. 2019). Hence, $a = 0.290$ and ${n_2}^4 H = 0.832$. Seven independent measurements for amorphous water formed after 32 minutes of exposure at 90 K gave $A_{\rm IP} = 0$ [$\int A_{\rm IP}(\tilde{\nu}) d\tilde{\nu} = 0$ (cm^{-1})] and ${n_2}^4 H A_{\rm OP} = 6.2 \pm 0.4 \times 10^{-5}$ at 3696 cm^{-1} [${n_2}^4 H \int A_{\rm OP}(\tilde{\nu}) d\tilde{\nu} = 8.4 \pm 0.4 \times 10^{-4}$ (cm^{-1})], considering amorphous water formed on both sides of the Si substrate. Therefore, σ is derived as $1.0 \pm 0.2 \times 10^{-18}$ cm^2 at 3696 cm^{-1} from Equation (11) by adopting $N = 3.3 \pm 0.6 \times 10^{13}$ molecules cm^{-2}. β is also derived as $1.4 \pm 0.3 \times 10^{-17}$ cm molecule^{-1} at $\tilde{\nu}$ = 3710–3680 cm^{-1} from Equation (12).

Table 1 summarizes band strength values for water. The present experimental values ($1.4 \pm 0.3 \times 10^{-17}$ cm molecule^{-1}) are in good agreement with a recent theoretical calculation by Maté et al. (1.2×10^{-17} cm molecule^{-1}; Maté et al. 2021). Although similar band strengths have been assumed between dangling and bulk OH bonds on and in ice, respectively (McCoustra & Williams 1996), the three-coordinated dangling-OH bonds show more than 1 order of magnitude smaller band strengths than bonds in bulk amorphous and crystalline ices and liquid water (Schaaf & Williams 1973; Mastrapa et al. 2009; Max & Chapados 2009). This indicates that the hydrogen-bonding networks in bulk ice and liquid water significantly enhance the IR absorption (Ohno et al. 2005; Gorai et al. 2020). Table 1 also shows the band strengths for the antisymmetric OH stretching vibration of H_2O monomers confined in solid matrices of CO, N_2, and O_2 (Ehrenfreund et al. 1996). The band strengths range from 3.3×10^{-18} cm molecule^{-1} to 1.1×10^{-17} cm molecule^{-1} depending on the solid matrices (Hujo et al. 2011; Maté et al. 2021), whereas these values are smaller than the band strength of the three-coordinated dangling-OH bonds ($1.4 \pm 0.3 \times 10^{-17}$ cm molecule^{-1}). This suggests that the dipole moment of a three-coordinated molecule at the amorphous water surface is enhanced by surrounding water molecules (Gregory et al. 1997; Hodgson & Haq 2009), which leads to an increase in the band strength of the three-coordinated dangling-OH bonds compared with H_2O monomers confined in solid matrices. To understand the effects of the hydrogen-bond coordination number, the absolute band strength of the two-coordinated dangling-OH bonds are necessary. More detailed investigation including measurements of σ and band strength for the two-coordinated dangling-OH bonds is in progress to clarify the surface structure and properties of interstellar ices.

This work was supported by JSPS Kakenhi grant Numbers 21H01143 and 21H05421.

Appendix

A.1. Low-temperature, Ultrahigh-vacuum IR–MAIRS Apparatus

Details of the experimental setup for low-temperature, ultrahigh-vacuum infrared multiple-angle incidence resolution spectrometry (IR–MAIRS) are described elsewhere (Hama et al. 2020). Hence, only a brief outline is given here. The apparatus consists of a vacuum chamber and a Fourier transform infrared (FT–IR) spectrometer. The chamber was evacuated to ultrahigh-vacuum conditions (base pressure 10^{-7} Pa at room temperature) using a turbo molecular pump (STP-451, Edwards). A Si(111) substrate ($40 \times 40 \times 1$ mm; Pier Optics Co., Ltd.) and a copper sample holder were connected with indium solder. The sample holder was connected to the cold head of a closed-cycle He refrigerator (RDK-101D, Sumitomo Heavy Industries) and installed in the vacuum chamber using a bore-through rotary feedthrough (KRP-152, Kitano Seiki Co., Ltd.). As the He refrigerator and Si substrate were freely rotatable by the rotary feedthrough, the angle of incidence of the IR beam (θ) could be varied by rotating the Si substrate within the accuracy of $\pm 0.^{\circ}5$. The Si substrate in the chamber was installed in the sample compartment of the FT–IR spectrometer (Nicolet iS50, Thermo Fisher Scientific) in transmission geometry across two ZnSe windows (3 mm in thickness) in the chamber. The temperature of the Si substrate was measured using a Si diode sensor (DT-670, Lakeshore) placed in the copper sample holder and controlled with an accuracy of $\pm$0.2 K using a temperature controller (Model 325, Lakeshore) and a ceramic heater (40 W).

Purified H_2O (resistivity $\geqslant$18.2 MΩ cm at 298 K) from a Millipore Milli-Q water purification system was mixed with

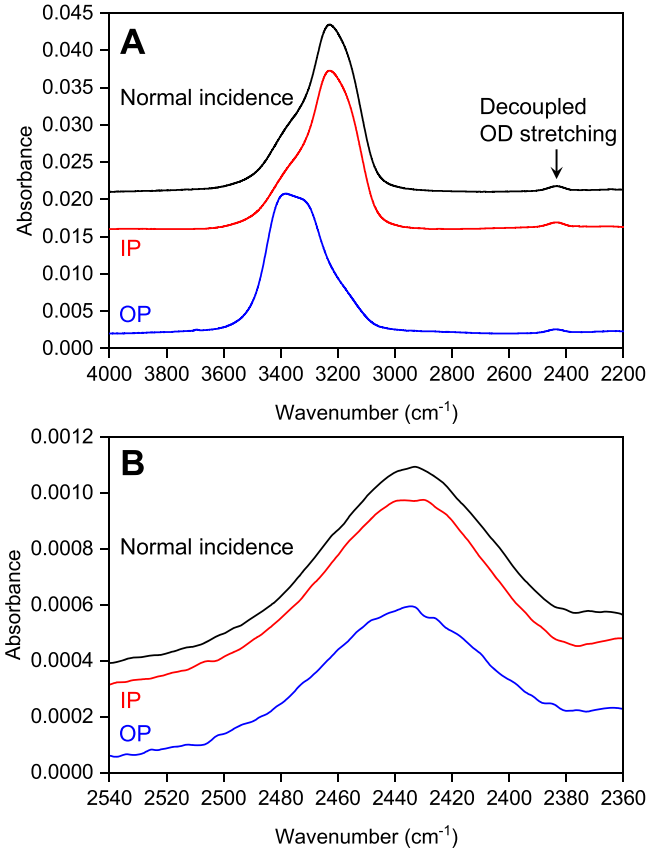

Figure 4. Normal-incidence ($\theta = 0°$, $\phi = 90°$), IP and OP spectra for amorphous water on a Si substrate at 90 K. (A) OH stretching vibrational region. (B) Decoupled OD stretching vibrational region. Amorphous water was prepared at 90 K by 32 minutes exposure of H_2O (with 3.5 mol% HDO) at 2.2×10^{-6} Pa. The IP and OP spectra's vertical axes (absorbance) are A_{IP} and $n_2^4 HA_{OP}$ in Equations (5) and (7), respectively, because they reflect k_{2xy} and k_{2z} with the common ordinate scale as $A_{IP}/\, n_2^4 HA_{OP} = k_{2xy}/k_{2z}$.

2.0 wt% (1.8 mol%) D_2O (deuteration degree >99.9%, Merck) to obtain a water sample containing about 3.5 mol% HDO with a negligible amount of D_2O. As described in the *IR–MAIRS measurements and analysis* section, the water sample containing HDO facilitated measurement of the OD stretching vibration of HDO molecules in the bulk ice decoupled from intramolecular and intermolecular OH stretching vibrations (Figure 4 in the Appendix of this article; Hama et al. 2017). The decoupled OD stretching vibration band was used to confirm the formation of amorphous ice, because its peak frequency is sensitive to the local lattice structure (oxygen–oxygen distance) in the ice (Franks 1972; Klug et al. 1987; Hama et al. 2017). For reference, crystalline ice I at 90 K shows a sharp single peak at 2417 cm^{-1} in the decoupled OD stretching vibrational region (Franks 1972; Hama et al. 2017). The contribution of the surface HDO molecules to dangling OH bonds should be negligible considering its small concentration of 3.5 mol%.

Water was first degassed by several freeze–pump–thaw cycles, and then background vapor deposited at $2.2^{+1.3}_{-0.6} \times 10^{-6}$ Pa to form amorphous water, which corresponds to a flux of $8.0^{+4.4}_{-2.1} \times 10^{12}$ molecules cm^{-2} s^{-1}. The pressure was measured using a cold cathode gauge (423 I-Mags® Cold Cathode Vacuum Sensor, MKS) and calculated using the gas correction factor for H_2O (1.25 ± 0.44) (Nakao 1975). Hence, amorphous water formed by vapor deposition for 32, 64, and 128 minutes corresponds to exposures of $1.5^{+0.8}_{-0.4} \times 10^{16}$, $3.1^{+1.7}_{-0.8} \times 10^{16}$, and $6.2^{+3.3}_{-1.6} \times 10^{16}$ molecules cm^{-2}, respectively. For reference, the lattice parameters of hexagonal ice indicate about 1.0×10^{15} molecules cm^{-2} on the surface (Petrenko & Whitworth 1999).

The methanol deposition experiments used CH_3OH (99%; Nacalai Tesque, Inc., Kyoto, Japan). The deposition pressure was calculated as $2.2 \pm 0.2 \times 10^{-8}$ Pa using the gas correction factor for CH_3OH (1.69–2.12) (Bartmess & Georgiadis 1983; Levis et al. 1989; Schulte et al. 1994). The flux of CH_3OH was estimated as $7.8 \pm 0.9 \times 10^{10}$ molecules cm^{-2} s^{-1}.

A.2. IR–MAIRS Measurements and Analysis

IR–MAIRS is well established for the molecular orientation analysis of organic thin films through measuring both the pure IP and OP vibration spectra. Recent articles and a textbook detail the measurement and analytical procedures of IR–MAIRS (Hasegawa 2017; Shioya et al. 2019; Hasegawa & Shioya 2020). In short, the angle of incidence (θ) was kept at 45° during measurements, which is the optimal angle for a Si substrate in IR–MAIRS (Shioya et al. 2019). The FT-modulated IR light was passed through an angle-controllable wire-grid linear ZnSe polarizer incorporated in the FT–IR spectrometer, and oblique incidence transmission measurements were taken at $\theta = 45°$ at seven polarization angles from $\phi = 0°$ (s-polarization) to 90° (p-polarization) in 15° steps. A mercury cadmium telluride detector detected the IR light, and the intensity of the transmitted IR light was measured as a single-beam measurement by the FT–IR (Shioya et al. 2019; Hama et al. 2020). The accumulation number of the single-beam measurements was 1000 (615 s) for each polarization angle with a resolution of 4 cm^{-1}. The total measurement time was 4305 s (72 min) for one IR–MAIRS measurement.

The intensity of the transmitted IR light measured as single-beam spectra ($\boldsymbol{s}_{obs}$) with polarization angle ϕ and incident angle θ (fixed at 45°) is expressed as a linear combination of the IP and OP polarization components ($\boldsymbol{s}_{IP}$ and $\boldsymbol{s}_{OP}$, respectively) with weighting ratios (r_{IP} and r_{OP}, respectively) and nonlinear noise factors $\boldsymbol{U}$ (e.g., reflected IR light).

$$\boldsymbol{s}_{obs} = r_{IP}\boldsymbol{s}_{IP} + r_{OP}\boldsymbol{s}_{OP} + \boldsymbol{U} \tag{A1}$$

The collection of the jth single-beam spectrum, $\boldsymbol{s}_{obs,j}$ ($j = 1$, 2, ..., 7), at a polarization angle of ϕ_j ($j = 1$, 2, ..., 7) forms the matrix, $\boldsymbol{S}$, and the linear combination part can be tied up using classical least-squares regression (Equation (A2)):

$$\begin{aligned}\boldsymbol{S} &= \begin{pmatrix} \boldsymbol{s}_{obs,1} \\ \boldsymbol{s}_{obs,2} \\ \vdots \\ \boldsymbol{s}_{obs,7} \end{pmatrix} \\ &= \begin{pmatrix} r_{IP,1} & r_{OP,1} \\ r_{IP,2} & r_{OP,2} \\ \vdots & \vdots \\ r_{IP,7} & r_{OP,7} \end{pmatrix} \begin{pmatrix} \boldsymbol{s}_{IP} \\ \boldsymbol{s}_{OP} \end{pmatrix} + \boldsymbol{U} \\ &\equiv \boldsymbol{R} \begin{pmatrix} \boldsymbol{s}_{IP} \\ \boldsymbol{s}_{OP} \end{pmatrix} + \boldsymbol{U} \end{aligned} \tag{A2}$$

where $\boldsymbol{R}$ is a matrix of weighting coefficients of $r_{IP,j}$ ($j = 1$, 2...7) and $r_{OP,j}$ ($j = 1$, 2 ...7) for $\boldsymbol{s}_{IP}$ and $\boldsymbol{s}_{OP}$, respectively. Itoh

et al. and Shioya et al. theoretically deduced $\boldsymbol{R}$ as

$$\boldsymbol{R} = \begin{pmatrix} \gamma\cos^2\phi_1 + \sin^2\phi_1(\sin^2\theta\tan^2\theta + \cos^2\theta) & \sin^2\phi_1\tan^2\theta \\ \gamma\cos^2\phi_2 + \sin^2\phi_2(\sin^2\theta\tan^2\theta + \cos^2\theta) & \sin^2\phi_2\tan^2\theta \\ \vdots & \vdots \\ \gamma\cos^2\phi_7 + \sin^2\phi_7(\sin^2\theta\tan^2\theta + \cos^2\theta) & \sin^2\phi_7\tan^2\theta \end{pmatrix}, \tag{A3}$$

where γ is the intensity ratio of the s-polarized light to the p-polarized light when measured without a substrate (Itoh et al. 2009; Shioya et al. 2019). $\boldsymbol{U}$ is a "garbage matrix" that receives the nonlinear responses to $\boldsymbol{R}$: that is, noise factors are rejected in the classical least-squares regression calculation and pooled in $\boldsymbol{U}$ as an error term. Equation (A2) means that $\boldsymbol{s}_{\rm IP}$ and $\boldsymbol{s}_{\rm OP}$ can be calculated as the least-squares solution of the classical least-squares regression equation as

$$\begin{pmatrix} \boldsymbol{s}_{\rm IP} \\ \boldsymbol{s}_{\rm OP} \end{pmatrix} = (\boldsymbol{R}^{\rm T}\boldsymbol{R})^{-1}\boldsymbol{R}^{\rm T}\boldsymbol{S}. \tag{A4}$$

After obtaining $\boldsymbol{s}_{\rm IP}$ and $\boldsymbol{s}_{\rm OP}$, the IP and OP absorbance spectra ($A^{\theta}_{\rm IP}$ and $A^{\theta}_{\rm OP}$, respectively) can be obtained as follows:

$$A^{\theta}_{\rm IP} = -\log_{10}\frac{\boldsymbol{s}^{s}_{\rm IP}}{\boldsymbol{s}^{b}_{\rm IP}} \tag{A5}$$

$$A^{\theta}_{\rm OP} = -\log\frac{\boldsymbol{s}^{s}_{\rm OP}}{\boldsymbol{s}^{b}_{\rm OP}}, \tag{A6}$$

where the superscripts b and s indicate background and sample measurements, respectively.

According to previous studies (Itoh et al. 2009; Shioya et al. 2019), $A^{\theta}_{\rm IP}$ originally corresponds to the s-polarized transmission spectrum measured at the incidence angle of θ.

$$A^{\theta}_{\rm IP} = \frac{8\pi da'}{\lambda\ln(10)}(2n_2k_{2xy}) \tag{A7}$$

$$a' = \frac{1}{n_1\cos\theta + n_3\cos\theta_3} + \left(\frac{n_1\cos\theta - n_3\cos\theta_3}{n_1\cos\theta + n_3\cos\theta_3}\right)^4 \times\left\{1 - \left(\frac{n_1\cos\theta - n_3\cos\theta_3}{n_1\cos\theta + n_3\cos\theta_3}\right)^4\right\}^{-1} \left(\frac{2n_3\cos\theta_3}{{n_3}^2 - {n_1}^2}\right), \tag{A8}$$

where n_1 and n_3 are the refractive indices of vacuum and the substrate, respectively. $n_1\sin\theta = n_3\sin\theta_3$, and thus, $n_3\cos\theta_3 = \sqrt{{n_3}^2 - (n_1\sin\theta)^2}$. $2n_2k_{2xy}$ is the TO energy-loss function, where n_2 and k_{2xy} are the real part and the x- and y-components (surface-parallel component) of the imaginary part of the complex refractive index of the thin sample (Figure 1 defines the x- and y-directions). Thus, absorbance correction is performed to make the IP spectrum quantitatively coincide with the normal-incidence transmission spectrum ($A^{\theta=0}_{\rm thin}$ in Equation (2) in the main text). This is easily done by calculating the intensity ratio of a/a'.

$$a = \frac{1}{n_1 + n_3} + \left(\frac{n_1 - n_3}{n_1 + n_3}\right)^4 \times\left\{1 - \left(\frac{n_1 - n_3}{n_1 + n_3}\right)^4\right\}^{-1}\left(\frac{2n_3}{{n_3}^2 - {n_1}^2}\right) \tag{A9}$$

$$\frac{a}{a'}A^{\theta}_{\rm IP} = \frac{8\pi da}{\lambda\ln 10}(2n_2k_{2xy}) = A^{\theta=0}_{\rm thin} = A_{\rm IP}. \tag{A10}$$

$A_{\rm IP}$ in Equation (A10) is identical to that in Equation (5) in the main text. In this study, $n_1 = 1$ for vacuum, $n_2 = 1.26$ for amorphous H_2O at 90 K (1.16 at 10 K) (Kofman et al. 2019), and $n_3 = 3.41$ for the Si substrate (Tasumi 2014; Shioya et al. 2019), and the values for a' and a were calculated as 0.3840 and 0.2896, respectively. Therefore,

$$\frac{a}{a'} = \frac{0.2896}{0.3840} = \frac{1}{1.326}. \tag{A11}$$

Shioya et al. confirmed experimentally that $\frac{a}{a'}A^{\theta}_{\rm IP}$ ($= A_{\rm IP}$) corresponds quantitatively to the normal-incidence transmission spectrum ($A^{\theta=0}_{\rm thin}$) (Shioya et al. 2019). We also confirmed that the IP spectrum ($\frac{a}{a'}A^{\theta}_{\rm IP} = A_{\rm IP}$) and normal-incidence spectrum ($A^{\theta=0}_{\rm thin}$) for amorphous water at 90 K formed by 32 minutes of vapor exposure have almost identical decoupled-OD stretching bands in terms of peak wavenumber (2433 $\rm cm^{-1}$ for both $A_{\rm IP}$ and $A^{\theta=0}_{\rm thin}$), height (0.00057 for $A_{\rm IP}$ and 0.00058 for $A^{\theta=0}_{\rm thin}$), width (61 $\rm cm^{-1}$ FWHM height for both $A_{\rm IP}$ and $A^{\theta=0}_{\rm thin}$), and area [0.0373 ($\rm cm^{-1}$) for $A_{\rm IP}$ and 0.0374 ($\rm cm^{-1}$) for $A^{\theta=0}_{\rm thin}$ at 2520–2376 $\rm cm^{-1}$) (Figure 4). This validates the IR–MAIRS measurements and analysis in the present study. For reference, the IP and OP spectra of amorphous water show substantially different band shapes in the OH stretching vibrational region (Figure 4). Because IR–MAIRS can obtain TO and LO energy-loss functions as IP and OP spectra, respectively, this IP − OP band shift originates from the TO − LO splitting, which is induced by the dispersion of n_2 induced by the large k_2 values, namely, the strong IR absorption in the OH stretching vibrational region (Mastrapa et al. 2009; Hama et al. 2020).

$A^{\theta}_{\rm OP}$ is expressed as follows with the LO energy-loss function, $2n_2k_{2z}/({n_2}^2 + {k_{2z}}^2)^2$(Itoh et al. 2009; Shioya et al. 2019):

$$A^{\theta}_{\rm OP} = \frac{8\pi da'}{H\lambda\ln 10}\frac{(2n_2k_{2z})}{({n_2}^2 + {k_{2z}}^2)^2}, \tag{A12}$$

where H is the substrate-specific correction factor (0.33 for Si) to account for the intensity ratio of the electric fields at the optical interface along the surface-parallel and surface-perpendicular directions (Shioya et al. 2019). Following the same absorbance correction, $A_{\rm OP}$ in Equation (6) in the main text is obtained.

$$\frac{a}{a'}A^{\theta}_{\rm OP} = \frac{8\pi da}{H\lambda\ln 10}\frac{(2n_2k_{2z})}{({n_2}^2 + {k_{2z}}^2)^2} = A_{\rm OP}. \tag{A13}$$

The base lines of the spectra in Figures 2 and 3 in the main text are corrected and offset for clarity. The IP and OP spectra's vertical axes (absorbance) are $A_{\rm IP}$ and $n_2^4 HA_{\rm OP}$ in Equations (5) and (7), respectively, because they reflect k_{2xy} and $k_{2z}$with the common ordinate scale as $A_{\rm IP}/\ n_2^4 HA_{\rm OP}\ = k_{2xy}/k_{2z}$.

A.3. The Number Density of CH_3OH Adsorbed on the Surface of Amorphous Water

The number density of CH_3OH adsorbed on the amorphous water surface is estimated from the C–O stretching band at 1033 cm^{-1} (Figure 3(B)). In our setup, the number density (N, molecules cm^{-2}) can be calculated by rearranging Equation (12) in the main text as follows.

$$N = \left(\frac{2}{3}\int A_{\rm IP}(\tilde{\nu})d\tilde{\nu} + \frac{{n_2}^4 H}{3}\int A_{\rm OP}(\tilde{\nu})d\tilde{\nu}\right) \times \frac{\ln 10}{4an_2\beta}. \quad \text{(A14)}$$

Equation (A14) shows that the number density of CH_3OH can be calculated from the IP and OP peak areas at $\tilde{\nu}\ =$ 1050–1020 cm^{-1} when the band strength β (integrated absorption cross section) is available. This study uses the band strength reported for amorphous CH_3OH ($\beta = 1.59$–$1.69\ \times\ 10^{-17}$ cm molecule^{-1}; Luna et al. 2018), considering a broad single peak at 1033 cm^{-1} (Figure 3(B)). Repeated experiments show that CH_3OH deposition for 6.5 ± 0.5 minutes is required to fully quench the peak. This corresponds to $\int A_{\rm IP}(\tilde{\nu})d\tilde{\nu} = 0$ (cm^{-1}) and ${n_2}^4 H\int A_{\rm OP}(\tilde{\nu})d\tilde{\nu}\ = 1.1 \pm 0.1 \times\ 10^{-3}$ (cm^{-1}), considering CH_3OH is adsorbed on both sides of the Si substrate. Hence, the number density of CH_3OH is estimated as $N = 3.5 \pm 0.4 \times 10^{13}$ molecules cm^{-2}. Because the coverage of CH_3OH (less than 0.1 monolayer) is much smaller than that of amorphous water (about 15 monolayers), the refractive index of amorphous water at 90 K (1.26) was used as a good approximation for n_2 (Kofman et al. 2019; Hama et al. 2020).

A.4. Band Strength Calculations for Crystalline Ice and Liquid Water

The band strengths for crystalline ice and liquid water in Table 1 in the main text are calculated using reported values for the imaginary part of the complex refractive index, $k(\tilde{\nu})$, at $\tilde{\nu}=$ 3900–2700 cm^{-1}. Schaaf and Williams reported values for crystalline ice at 267 K (Schaaf & Williams 1973), and Max and Chapados gave values for liquid water at 295 K (Max & Chapados 2009). The absorption coefficients (α, cm^{-1}) at $\tilde{\nu}=$ 3900–2700 cm^{-1} are calculated from $k(\tilde{\nu})$:

$$\alpha(\tilde{\nu}) = 4\pi k(\tilde{\nu})\tilde{\nu}. \quad \text{(A15)}$$

Considering the densities of crystalline ice ($D = 0.91668$ g cm^{-3} at 273 K) and liquid water ($D = 0.99708$ g cm^{-3} at 298 K) (Kell 1967; Petrenko & Whitworth 1999), the mean molecular mass of H_2O ($M_{H_2O} = 18.015$ g mol^{-1}) (Petrenko & Whitworth 1999), and Avogadro's constant ($N_A = 6.0221 \times\ 10^{23}$ mol^{-1}) (Petrenko & Whitworth 1999), the absorption cross sections (σ, cm^2) at a given wavenumber ($\tilde{\nu}$) can be derived as

$$\sigma(\tilde{\nu}) = \frac{M_{H_2O}\alpha(\tilde{\nu})}{DN_A}. \quad \text{(A16)}$$

The band strength β (cm molecule^{-1}) is obtained by integrating $\sigma(\tilde{\nu})$ at $\tilde{\nu}=$ 3900–2700 cm^{-1}.

$$\beta = \int \sigma(\tilde{\nu})d\tilde{\nu}. \quad \text{(A17)}$$

ORCID iDs

Naoki Numadate https://orcid.org/0000-0001-8992-0812
Nobutaka Shioya https://orcid.org/00000002-2915-894X
Takafumi Shimoaka https://orcid.org/00000001-9131-9831
Takeshi Hasegawa https://orcid.org/00000001-5574-9869
Tetsuya Hama https://orcid.org/0000-0002-4991-4044

References

Bahr, S., Toubin, C., & Kempter, V. 2008, JChPh, 128, 134712
Bartmess, J. E., & Georgiadis, R. M. 1983, Vacuu, 33, 149
Bu, C., Shi, J., Raut, U., Mitchell, E. H., & Baragiola, R. A. 2015, JChPh, 142, 134702
Buch, V., & Devlin, J. P. 1991, JChPh, 94, 4091
Dawes, A., Mason, N. J., & Fraser, H. J. 2016, PCCP, 18, 1245
Devlin, J. P., & Buch, V. 1995, JPhCh, 99, 16534
Ehrenfreund, P., Gerakines, P. A., Schutte, W. A., van Hemert, M. C., & van Dishoeck, E. F. 1996, A&A, 312, 263
Franks, F. 1972, Water a Comprehensive Treatise: Volume 7: Water and Aqueous Solutions at Subzero Temperatures (New York: Plenum Press)
Gorai, P., Sil, M., Das, A., et al. 2020, ESC, 4, 920
Gregory, J. K., Clary, D. C., Liu, K., Brown, M. G., & Saykally, R. J. 1997, Sci, 275, 814
Hagen, W., Tielens, A. G. G. M., & Greenberg, J. M. 1981, CP, 56, 367
Hama, T., Ishibashi, A., Kouchi, A., et al. 2020, J. Phys. Chem., 11, 7857
Hama, T., Ishizuka, S., Yamazaki, T., et al. 2017, PCCP, 19, 17677
Hama, T., & Watanabe, N. 2013, ChRv, 113, 8783
Hasegawa, T. 2017, Quantitative Infrared Spectroscopy for Understanding of a Condensed Matter (Tokyo: Springer)
Hasegawa, T., & Shioya, N. 2020, Bull. Chem. Soc. Jpn., 93, 1127
He, J., Clements, A. R., Emtiaz, S. M., et al. 2019, ApJ, 878, 94
Hodgson, A., & Haq, S. 2009, SurSR, 64, 381
Hujo, W., Gaus, M., Schultze, M., et al. 2011, JPCA, 115, 6218
Itoh, Y., Kasuya, A., & Hasegawa, T. 2009, JPCA, 113, 7810
Kell, G. S. 1967, J. Chem. Eng. Data, 12, 66
Klug, D. D., Mishima, O., & Whalley, E. 1987, JChPh, 86, 5323
Kofman, V., He, J., Loes ten Kate, I., & Linnartz, H. 2019, ApJ, 875, 131
Levis, R. J., Zhicheng, J., & Winograd, N. 1989, JAChS, 111, 4605
Luna, R., Molpeceres, G., Ortigoso, J., et al. 2018, A&A, 617, A116
Mastrapa, R. M., Sandford, S. A., Roush, T. L., Cruikshank, D. P., & Dalle Ore, C. M. 2009, ApJ, 701, 1347
Maté, B., Satorre, M., & Escribano, R. 2021, PCCP, 23, 9532
Max, J. J., & Chapados, C. 2009, JChPh, 131, 184505
McCoustra, M., & Williams, D. A. 1996, MNRAS, 279, L53
Nakao, F. 1975, Vacuu, 25, 431
Noble, J. A., Michoulier, E., Aupetit, C., & Mascetti, J. 2020, A&A, 644, A22
Ohno, K., Okimura, M., Akai, N., & Katsumoto, Y. 2005, PCCP, 7, 3005
Petrenko, V. F., & Whitworth, R. W. 1999, Physics of Ice, 1999 (New York: Oxford Univ. Press)
Schaaf, J. W., & Williams, D. 1973, JOSA, 63, 726
Schulte, M., Schlosser, B., & Seidel, W. 1994, AnaCh, 348, 778
Shioya, N., Fujiwara, R., Tomita, K., Shimoaka, T., & Hasegawa, T. 2020, JPCA, 124, 2714
Shioya, N., Tomita, K., Shimoaka, T., & Hasegawa, T. 2019, JPCA, 123, 7177
Stevenson, K. P., Kimmel, G. A., Dohnálek, Z., Smith, R. S., & Kay, B. D. 1999, Sci, 283, 1505
Tasumi, M. 2014, Introduction to Experimental Infrared Spectroscopy: Fundamentals and Practical Methods (Chichester: Wiley)
Umemura, J., Kamata, T., Kawai, T., & Takenaka, T. 1990, JPhCh, 94, 62
Van Dishoeck, E. F., Herbst, E., & Neufeld, D. A. 2013, ChRv, 113, 9043